The Very Low Barrier of CO Site Exchange in Tricarbonyl(η^4-1,5-cyclooctadiene)iron: Picosecond Kinetics in Solution Investigated by Line Shape Simulation of the ν(CO) IR Bands and Complementary Evidence from the Course of ^{13}CO Incorporation in a Low-Temperature Matrix

Friedrich-Wilhelm Grevels,*,† Klaus Kerpen,† Werner E. Klotzbücher,† R. E. D. McClung,*,‡ Graham Russell,† Manuella Viotte,† and Kurt Schaffner†

Contribution from the Max-Planck-Institut für Strahlenchemie, D-45413 Mülheim an der Ruhr, Germany, and the Department of Chemistry, University of Alberta, Edmonton, AB T6G 2G2, Canada

Received November 13, 1997

Abstract: Photochemical experiments with Fe(CO)$_3$(η^4-1,5-cyclooctadiene) (**1**) in a ^{13}CO matrix at 10 K, monitored by means of IR spectroscopy, indicate the generation of stereoselectively labeled Fe(CO)$_2$(^{13}CO)-(η^4-1,5-cyclooctadiene) (**1**-*1a*), with ^{13}CO in the apical position of the square-pyramidal coordination geometry. The spectral changes occurring upon annealing the matrix to 28 K reveal the thermally activated conversion into a mixture of the two possible stereoisotopomers, the species with ^{13}CO in a basal position (**1**-*1b*) becoming predominant. These findings characterize the carbonyl ligand site exchange in complex **1** as a chemical reaction involving a very small barrier. The variable-temperature IR spectra of **1** in hydrocarbon solution exhibit broadening and coalescence of bands in the ν(CO) region, which is interpreted in terms of a CO site exchange occurring in the picosecond time domain. The theoretical approach to the simulation of these spectral changes involves a transfer of transition dipole moment between the ν(CO) modes. On the basis of this approach, the rates of CO site exchange at the various temperatures could be evaluated by line shape simulation. They were found to range from 0.15×10^{12} s^{-1} at 133 K to 1.54×10^{12} s^{-1} at 293 K, yielding $\Delta H^{\ddagger} = 0.7$ kcal·mol^{-1} (Eyring plot) and $E_a = 1.1$ kcal·mol^{-1} (Arrhenius plot) for the activation barrier of the underlying process.

Introduction

Broadening and coalescence of CO stretching vibrational bands has been observed in the variable-temperature IR spectra of the tricarbonyl(η^4-diene)iron complexes **1** (diene = 1,5-cyclooctadiene; 1,5-cod) and **2** (diene = norbornadiene; nbd) and a few other, related compounds.[1−5]

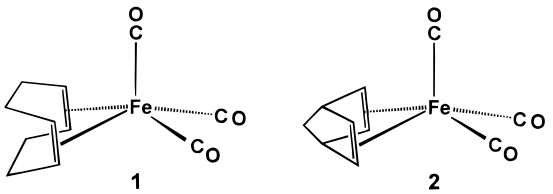

These spectral changes, illustrated in Figure 1 for the example of the norbornadiene complex **2**,[2] were interpreted in terms of a low-barrier, very fast site exchange of the CO ligands[6] in the apical and basal positions of the square-pyramidal coordination geometry, presumably proceeding via the turnstile rotation mechanism. In support of this notion, the temperature dependent changes in the ν(CO) pattern of a ^{13}CO-enriched[7] sample[4] of **2**

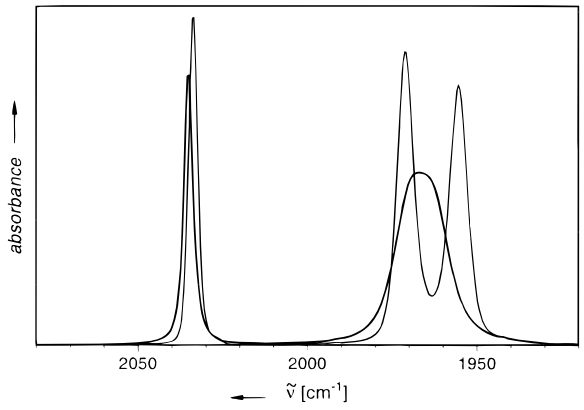

Figure 1. The ν(CO) bands in the IR spectrum of Fe(CO)$_3$(η^4-nbd) (**2**) recorded in 2-methylpentane solution[2] at 293 K (bold line) and 133 K.

* To whom correspondence should be addressed.
† Max-Planck-Institut für Strahlenchemie.
‡ University of Alberta.

(1) Grevels, F.-W.; Jacke, J.; Klotzbücher, W. E.; Krüger, C.; Seevogel, K.; Tsay, Y.-H. *Angew. Chem.* **1987**, *99*, 960−961; *Angew. Chem., Int. Ed. Engl.* **1987**, *26*, 885−887.

(2) Grevels, F.-W.; Jacke, J.; Seevogel, K. *J. Mol. Struct.* **1988**, *174*, 107−112.

(3) Jacke, J. Doctoral Dissertation, Max-Planck-Institut für Strahlenchemie/Universität-Gesamthochschule Duisburg, 1989.

(4) Turner, J. J.; Grevels, F.-W.; Howdle, S. M.; Jacke, J.; Haward, M. T.; Klotzbücher, W. E. *J. Am. Chem. Soc.* **1991**, *113*, 8347−8353.

(5) Grevels, F.-W.; McClung, R. E. D.; Russell, G.; Schrickel, J.; Takats, J. *Inorganic Reactions Mechanisms Meeting 93*; Wiesbaden, Germany, 1993; Abstract P22.

(6) The temperature-dependent IR ν(CO) pattern of Os$_4$(CO)$_{14}$ has also been suggested to arise from a degenerate rearrangement involving very fast CO site exchange: Johnston, V. J.; Einstein, F. W. B.; Pomeroy, R. K. *Organometallics* **1988**, *7*, 1867−1869.

S0002-7863(97)03897-3 CCC: $15.00
Published on Web 09/19/1998

Scheme 1

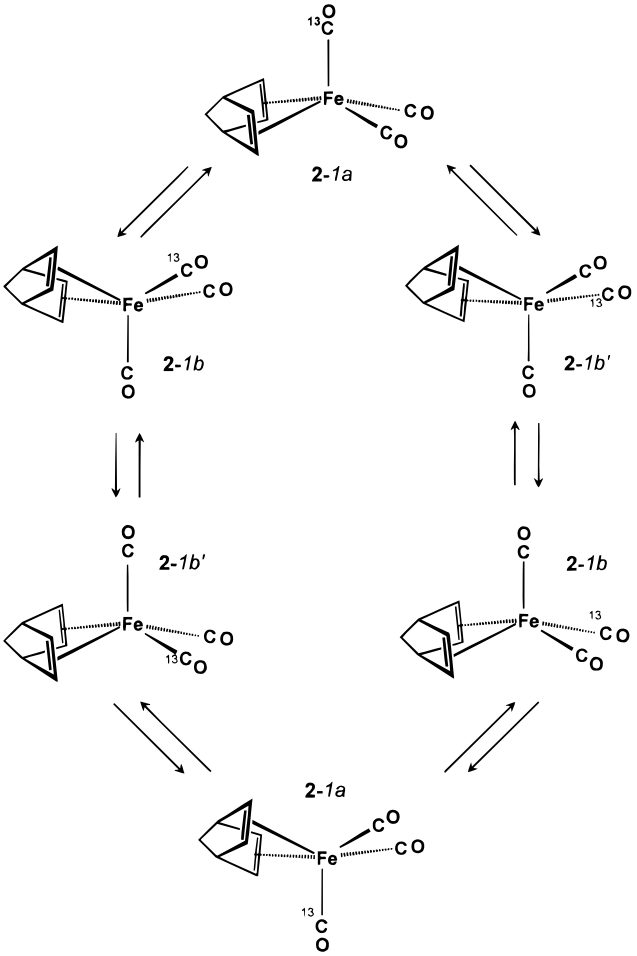

proved consistent with an equally rapid interconversion of positional isotopomers (CO/^{13}CO site exchange), as sketched out in Scheme 1 for the case of the monolabeled species Fe(CO)$_2$(^{13}CO)(η^4-nbd) carrying the ^{13}CO group in the apical (**2**-*1a*) or a basal (**2**-*1b*/**2**-*1b′*) position.[7]

Similar vibrational line broadening phenomena, although generally less well pronounced, have been previously reported for systems undergoing proton-transfer reactions, rotations about single bonds, and other very fast reversible processes thought to occur in the picosecond time domain. It is appealing to exploit these changes in the band profiles, recorded at leisure by conventional spectroscopic means, for the purpose of evaluating picosecond kinetic data under equilibrium conditions,[8−13] in imitation of the well-established methods of dynamic NMR spectroscopy.[14,15]

However, the validity of this conception has been challenged,[16] whereby the objections have focused on the problem of separating the effects of the reactive motion across a barrier along the reaction coordinate (interwell dynamics) from those of nonreactive motion within a potential well (intrawell dynamics), which both may give rise to temperature-dependent spectral changes. Moreover, it was argued that the implicit condition of a very short transit time across the barrier, compared with the lifetime in a potential well, might be violated in the case of picosecond lifetimes.

For the particular case of complex **2** an alternative model was launched,[17] adapted from a similar treatment of the methyl C−H stretching vibrations in linear alkanes.[18] This model aims at the rationalization of the ν(CO) band coalescence (Figure 1) exclusively in terms of intrawell dynamics, i.e., without a rapid site exchange of the carbonyl ligands. To this end, the three-band ν(CO) pattern of **2** (2 *A′*, A″; Cs symmetry) in the low-temperature spectrum was interpreted in terms of the ν(CO) force field of an Fe(CO)$_3$ skeleton with C_{3v} symmetry [two CO stretching modes (A_1, E); one principal CO force constant and one interaction force constant], to which the effect of the norbornadiene ligand was added in the form of a Hamiltonian accounting for the torsional motion of the diene relative to the Fe(CO)$_3$ moiety. In this way, the degenerate ν(CO) E mode should split into two components, the gradual collapse of which was suggested to result from the increasing amplitude of the torsional motion upon raising the temperature. However, a recent density functional study of **2** indicates that the separation of those two ν(CO) modes is almost independent of the torsional angle between the Fe(CO)$_3$ unit and the norbornadiene ligand,[19] which invalidates the key feature of the above model. Noted with great interest, the turnstile rotational barrier associated with the CO site exchange in **2** was computed, in the same study,[19] to be indeed as low as 0.5 kcal·mol^{-1}. Moreover, a recent thorough discussion,[20] based on a careful reexamination of the ν(CO) band profiles of **2**, led to the conclusion that the details of the spectral changes with temperature cannot be explained by a mechanism without a rapid site exchange of the carbonyl ligands.

Concerning the ν(CO) band splittings arising from ^{13}CO isotopic substitution in either the apical or a basal position of **2**, the outline of the aforementioned model[17] offered merely a qualitative discussion. It was concluded that the isotope splittings should collapse, upon raising the temperature, in about the same way as the splitting in the isotopically pure complex **2**, i.e., as a result of intrawell dynamics.

In our present study, ^{13}CO-labeling experiments with complex **1** in a low-temperature matrix provide clear evidence of the existence of the positional isotopomers as distinct molecules, separated by a very small barrier on the potential energy surface.

(7) Note that throughout this paper CO = ^{12}C^{16}O and ^{13}CO = ^{13}C^{16}O. In the numbering scheme for ^{13}CO substituted Fe(CO)$_3$(η^4-diene) complexes the characters printed in italics refer to the number of ^{13}CO groups (*1*, *2*, or *3*) and their position (*a* = apical, *b* = basal) in the square-pyramidal structure. The symbol # designates a mixture of isotopomeric molecules with statistical distribution of ^{13}CO.

(8) (a) Kreevoy, M. M.; Mead, C. A. *J. Am. Chem. Soc.* **1962**, *84*, 4596−4597. (b) Kreevoy, M. M.; Mead, C. A. *Discuss. Faraday Soc.* **1965**, *39*, 166−171.

(9) MacPhail, R. A.; Snyder, R. G.; Strauss, H. L. *J. Am. Chem. Soc.* **1980**, *102*, 3976.

(10) Cohen, B.; Weiss, S. *J. Phys. Chem.* **1983**, *87*, 3606−3610.

(11) Strehlow, H.; Wagner, I.; Hildebrandt, P. *Ber. Bunsenges. Phys. Chem.* **1983**, *87*, 516−522.

(12) Strehlow, H. *Rapid Reactions in Solution*; VCH Verlagsgesellschaft: Weinheim, Germany, 1992; Chapter 7.2, pp 199−206.

(13) Related studies by other authors (A. K. Covington et al., R. E. Weston, D. E. Irish et al., J. Lascombe et al., S. Bratos et al.) and further publications by M. M. Kreevoy et al., H. Strehlow et al., and B. Cohen et al. are cited in refs 10, 12, and 16.

(14) (a) Sandström, J. *Dynamic NMR Spectroscopy*; Academic Press: London, 1982. (b) Günther, H. *NMR−Spektroskopie*; Georg Thieme Verlag: Stuttgart, 1983.

(15) For a comparative discussion of the accessible time ranges for measuring the kinetics of reversible processes on the basis of line broadening and coalescence in NMR (1−10^{-5} s), EPR (10^{-5}−10^{-10} s), and vibrational (<10^{-11} s) spectroscopy see ref 12, chapters 6 and 7.

(16) (a) MacPhail, R. A.; Strauss, H. L. *J. Chem. Phys.* **1985**, *82*, 1156−1166. (b) Wood, K. A.; Strauss, H. L. *Ber. Bunsen-Ges. Phys. Chem.* **1989**, *93*, 615−616. (c) Wood, K. A.; Strauss, H. L. *J. Phys. Chem.* **1990**, *94*, 5677−5684.

(17) Strauss, H. L. *J. Am. Chem. Soc.* **1992**, *114*, 905−907.

(18) MacPhail, R. A.; Snyder, R. G.; Strauss, H. L. *J. Chem. Phys.* **1982**, *77*, 1118−1137.

(19) Bühl, M.; Thiel, W. *Inorg. Chem.* **1997**, *36*, 2922−2924.

(20) Turner, J. J.; Gordon, C. M.; Howdle, S. M. *J. Phys. Chem.* **1995**, *99*, 17532−17538.

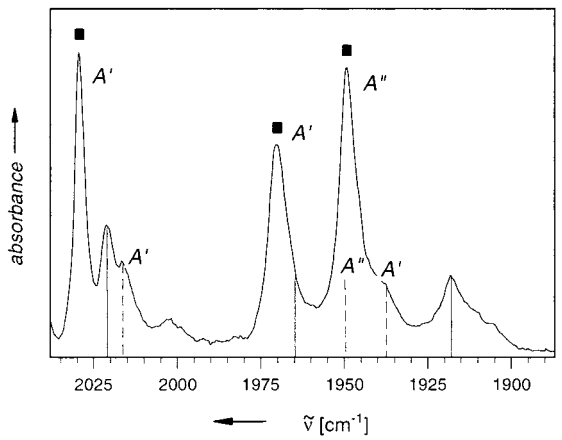

Figure 2. The ν(CO) bands in the IR spectrum of $Fe(CO)_{3-n}(^{13}CO)_n$(η^4-1,5-cod) (**1**-#; $n = 0$, 54%; $n = 1$, 37%; $n = 2$, 8%)[21] recorded in a ^{13}CO matrix at 10 K. The symbols and vertical lines, respectively, refer to the unlabeled complex **1** (■) and to the two monolabeled positional isotopomers **1**-*1a* (- - -) and **1**-*1b* (—) carrying the ^{13}CO label in the apical or a basal position (cf. Table 1).

This experimental result, along with the aforementioned theoretical findings,[19,20] encouraged us again to take up the idea that the temperature dependence of the ν(CO) band profiles in the IR spectra of complexes such as **1** and **2** does indeed reflect a low-barrier CO site exchange occurring in the picosecond time domain. Thus, we set about to attempt line shape simulations, based on the notion of transition dipole moment transfer between the various ν(CO) modes and aiming at the elucidation of the picosecond kinetic data, from which the activation barrier for the underlying process can be determined.

Results and Discussion

Isotopic Substitution of $Fe(CO)_3(\eta^4$-1,5-cod) (1) in a ^{13}CO Matrix. In accord with the C_s symmetry of $Fe(CO)_3(\eta^4$-1,5-cod) (**1**),[1] the low-temperature IR spectra in various matrices[21] exhibit three well-resolved bands in the CO stretching vibrational region (2 *A′*, *A″*). The treatment of this pattern on the basis of the energy-factored CO force field approximation[22] involves two principal force constants associated with the apical and basal CO groups (k_a, k_b) and two interaction force constants (k_{ab}, k_{bb}). Thus, additional frequency information from isotopically substituted derivatives is required to determine the complete set of CO force field parameters.

A ^{13}CO-enriched sample of **1**, $Fe(CO)_{3-n}(^{13}CO)_n(\eta^4$-1,5-cod) (**1**-#),[7] generated by irradiation of the complex in ^{13}CO-saturated solution and separated from concomitantly formed $Fe(CO)_{3-n}(^{13}CO)_n(\eta^4$-1,3-cod), was available from previous investigations into the photolytic behavior of **1**.[21] The spectrum displayed in Figure 2 shows the ν(CO) pattern of **1**-#, deposited in a ^{13}CO matrix at 10 K. The sample contains the unlabeled parent complex **1** as the major component (54%, $n = 0$) along with the monolabeled derivative **1**-*1* (37%, $n = 1$) and minor quantities of **1**-*2* (8%, $n = 2$) and **1**-*3* (1%, $n = 3$), as determined by mass spectrometry.[21] Accordingly, the spectrum is dominated by the three CO stretching vibrational bands of **1** (2029.5, 1970.2, and 1949.5 cm^{-1}), but several features associated with **1**-*1* are also clearly observable. Essential information on **1**-*1* comes from the two high-frequency ^{13}CO satellite bands at 2021.3 and 2016.4 cm^{-1}, which indicate that two different monolabeled isotopomers are present, **1**-*1a* and **1**-*1b*, carrying the ^{13}CO ligand in either the apical or a basal position. The latter isotopomer is statistically favored by a factor of 2,[23] such that the band of higher intensity is readily assigned to the species **1**-*1b*. The frequency data are collected in Table 1, along with the four CO force field parameters ($k_a = 1610.3$, $k_b = 1578.2$, $k_{ab} = 33.7$, and $k_{bb} = 43.0$ N m^{-1}) and the ν(CO) normal coordinates calculated therefrom. Comparison of the complete set of calculated frequencies (Table 1) with the pattern displayed in Figure 2 identifies the low-frequency *A′* mode of **1**-*1a* at 1938 cm^{-1} as a shoulder in the experimental spectrum.

Table 1. The CO Stretching Vibrations of $Fe(CO)_3(\eta^4$-1,5-cod) (**1**) and Its ^{13}CO Monolabeled Isotopomers in the IR Spectrum of a Statistically ^{13}CO-Enriched Sample (1-#)[7,21] Recorded in a ^{13}CO Matrix at 10 K

	$\tilde{\nu}$(CO) [cm^{-1}]			
complex	obsd	calcd[b]	ν(CO) normal coordinates[a]	
1 (C_s)	2029.5	2029.7	Q_1 (*A′*) =	$0.6659r_1 + 0.5275r_2 + 0.5275r_3$
	1970.2	1970.3	Q_2 (*A′*) =	$0.7461r_1 - 0.4708r_2 - 0.4708r_3$
	1949.5	1949.8	Q_3 (*A″*) =	$0.7071r_2 - 0.7071r_3$
1-*1a* (C_s)	2016.4	2016.4	Q_1 (*A′*) =	$0.4080r_1 + 0.6456r_2 + 0.6456r_3$
	(—)[c]	1949.8	Q_2 (*A″*) =	$0.7071r_2 + 0.7071r_3$
	(—)[c]	1938.1	Q_3 (*A′*) =	$0.9130r_1 - 0.2885r_2 - 0.2885r_3$
1-*1b* (C_1)[d]	2021.3	2021.2	Q_1 (*A*) =	$0.7586r_1 + 0.3389r_2 + 0.5564r_3$
	(—)[c]	1965.7	Q_2 (*A*) =	$-0.6353r_1 + 0.1953r_2 + 0.7472r_3$
	1918.1	1917.8	Q_3 (*A*) =	$-0.1446r_1 + 0.9203r_2 - 0.3635r_3$
1-*1b′* (C_1)[e]	2021.3	2021.2	Q_1 (*A*) =	$0.7586r_1 + 0.5564r_2 + 0.3389r_3$
	(—)[c]	1965.7	Q_2 (*A*) =	$-0.6353r_1 + 0.7472r_2 + 0.1953r_3$
	1918.1	1917.8	Q_3 (*A*) =	$-0.1446r_1 - 0.3635r_2 + 0.9203r_3$

[a] Notations r_1, r_2, and r_3 refer to the internal CO stretching coordinates in positions 1 (apical), 2 (basal), and 3 (basal). [b] CO force field parameters: $k_a = 1610.3$, $k_b = 1578.2$, $k_{ab} = 33.7$, $k_{bb} = 43.0$ N m^{-1}; the effective value for $\sqrt{\mu(^{12}C^{16}O)/\mu(^{13}C^{16}O)} = 0.9772$, employed in this calculation, is adopted from $Fe(CO)_3(\eta^4$-1,3-butadiene).[42] [c] Blank entries refer to bands hidden underneath more prominent absorptions. [d] ^{13}CO label in position 2. [e] ^{13}CO label in position 3.

Scheme 2

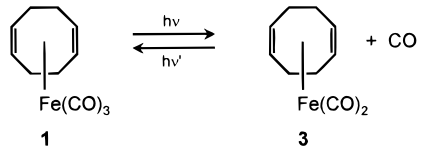

In this context it should be emphasized that a wide variety of other $Fe(CO)_3(\eta^4$-diene) compounds,[24] not exhibiting any temperature-dependent behavior, show the same ordering of the CO force field parameters ($k_a > k_b$, $k_{ab} < k_{bb}$) as derived above for **1** in the low-temperature matrix. A similar result was obtained for $Fe(CO)_3(\eta^4$-nbd) (**2**) in low-temperature solution,[4] such that the energy-factored CO force field approximation seems indeed adequate for **1** and **2**.

The photolysis of **1** in low-temperature matrices reportedly[21] generates the $Fe(CO)_2(\eta^4$-1,5-cod) fragment **3** as the only detectable product. This process, Scheme 2, is photoreversible, particularly in the presence of added CO, whereby longer wavelengths favor the recombination.

Analogous experiments in a ^{13}CO matrix now reveal that the addition of isotopically labeled carbon monoxide from the matrix

(21) Grevels, F.-W.; Klotzbücher, W. E.; Russell, G.; Schaffner, K. *Recl. Trav. Chim. Pays-Bas* **1995**, *114*, 571−576.

(22) (a) Braterman, P. S. *Metal Carbonyl Spectra*; Academic Press: London, 1975. (b) Cotton, F. A.; Kraihanzel, C. S. *J. Am. Chem. Soc.* **1962**, *84*, 4432−4438.

(23) Note that there are actually two species carrying the ^{13}CO group in a basal position, **1**-*1b* and **1**-*1b′* (cf. the related norbornadiene complex in Scheme 1). However, these two species are enantioisotopomers which give rise to identical ν(CO) spectra.

(24) (a) Warren, J. D.; Clark, R. J. *Inorg. Chem.* **1970**, *9*, 373−379. (b) Warren, J. D.; Busch, M. A.; Clark, R. J. *Inorg. Chem.* **1972**, *11*, 452−457. (c) Busch, M. A.; Clark, R. J. *Inorg. Chem.* **1975**, *14*, 219−225.

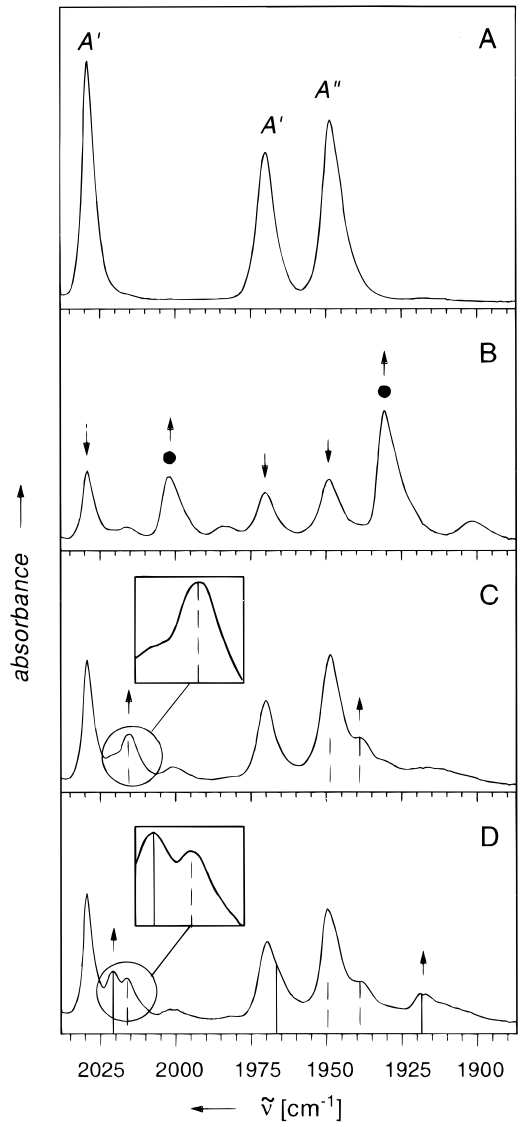

Figure 3. IR spectra in the ν(CO) region from an experiment with Fe(CO)$_3$(η^4-1,5-cod) (**1**) in a ^{13}CO matrix. (A) After deposition at 10 K. (B) After irradiation at λ_{exc} = 365 nm for 20 min, generating the Fe(CO)$_2$(η^4-1,5-cod) fragment (**3**, ●). (C) After subsequent irradiation through a 495 nm cutoff filter for 2 min, leading to incorporation of ^{13}CO with formation of apically labeled Fe(CO)$_2$(^{13}CO)(η^4-1,5-cod) (**1**-*1a*, - - -). (D) After subsequent annealing of the matrix to 28 K, indicating the appearance of the positional isotopomer **1**-*1b* (—). Arrows indicate the most significant changes in intensity.

environment to the dicarbonyl fragment **3** occurs with a high degree of stereoselectivity, as it yields almost exclusively one particular positional isotopomer of the Fe(CO)$_2$(^{13}CO)(η^4-1,5-cod) complex, viz., the species **1**-*1a* that carries the ^{13}CO group in the apical position. In detail, Figures 3A and 3B illustrate the generation of **3** [ν(CO) = 2003.5 and 1932 cm^{-1}] from **1** upon irradiation at λ_{exc} = 365 nm. The photolysis was stopped at ca. 60% conversion of the starting material, when the first signs of ^{13}CO incorporation into both the tricarbonyl complex and the dicarbonyl fragment [**3**-*1*: ν(CO) = 1984.5 and 1902 cm^{-1}] became just recognizable. Subsequent long-wavelength irradiation of the matrix through a 495 nm cutoff filter (Figure 3C) results in both the partial recovery of the unlabeled starting material **1** and the formation of a ^{13}CO-labeled derivative. In other words, despite the large excess of ^{13}CO in the bulk matrix, the re-coordination of photodissociated CO from the matrix cage competes efficiently with the take-up of ^{13}CO from the matrix

Scheme 3

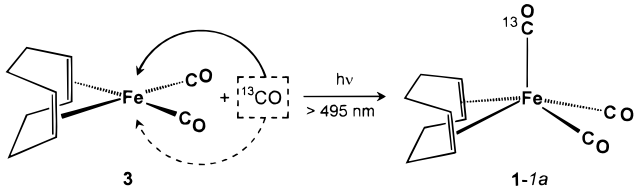

Scheme 4

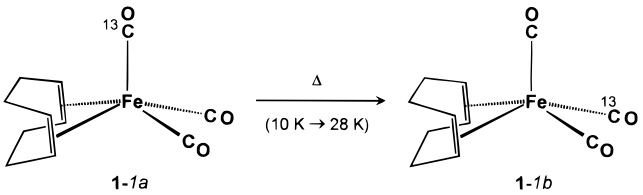

environment. This behavior parallels similar observations made with the fragment **3** in an N_2 matrix.[21]

The stereoselective incorporation of ^{13}CO is evident from the appearance of a band at 2016 cm^{-1} and a shoulder around 1938 cm^{-1} (Figure 3C), both of which are associated with the apically labeled species **1**-*1a* (Table 1), while absorptions of the second positional isotopomer **1**-*1b* are just barely discernible. The third CO stretching vibration of **1**-*1a*, expected at 1949.8 cm^{-1} (*A*″), is hidden underneath the coinciding *A*″ band of the parent complex **1**, the relative intensity of which is, however, accordingly increased.

These findings suggest a square-planar geometry for the structure of the dicarbonyl fragment **3**, since the approach from either the top or the bottom side brings the incoming ^{13}CO ligand directly into the apical position of the resulting tricarbonyl product (**1**-*1a*), Scheme 3.

Once generated as described above, the apically labeled species **1**-*1a* persists in the dark as long as the matrix temperature is maintained at 10 K. However, raising the temperature leads to gradual changes in the ν(CO) pattern which indicate the partial conversion of **1**-*1a* into the other positional isotopomer **1**-*1b*, Scheme 4. The spectrum displayed in Figure 3D illustrates the situation after annealing the matrix to 28 K, while the onset of this process became noticeable already at ca. 15 K. Two bands associated with **1**-*1b* grow in at 2021 and 1918 cm^{-1}, while the expected third band around 1966 cm^{-1} (cf. Table 1) merely gives rise to a weak shoulder on the low-frequency side of the *A*′ vibration of the unlabeled complex **1**.

It is evident from these observations that the two positional isotopomers of Fe(CO)$_2$(^{13}CO)(η^4-1,5-cod), **1**-*1a* and **1**-*1b*, exist as two distinct molecules. Moreover, the occurrence of the ^{13}CO/CO site exchange, **1**-*1a* → **1**-*1b* (Scheme 4), as a thermally activated process at temperatures as low as ≤28 K suggests a very low barrier between the potential wells along the reaction coordinate which, naturally, should be equally low for the CO site exchange in the case of the unlabeled complex **1**.

Variable-Temperature IR Spectra of Fe(CO)$_3$(η^4-1,5-cod) (1) and Fe(CO)$_3$(η^4-1,3-butadiene) (4). The spectra displayed in Figure 4, recorded in 2-methylpentane solution at temperatures ranging from 133 to 293 K, illustrate the dramatic changes with temperature in the IR ν(CO) pattern of **1**. The two bands at lower frequencies, associated with the out-of-phase *A*′ and *A*″ ν(CO) modes, gradually broaden, move together, and eventually collapse around ambient temperature, while the in-phase *A*′ ν(CO) band at higher frequency is much less affected.

The low-temperature (133 K) spectrum of **1** was closely examined to characterize the profiles of the three bands under

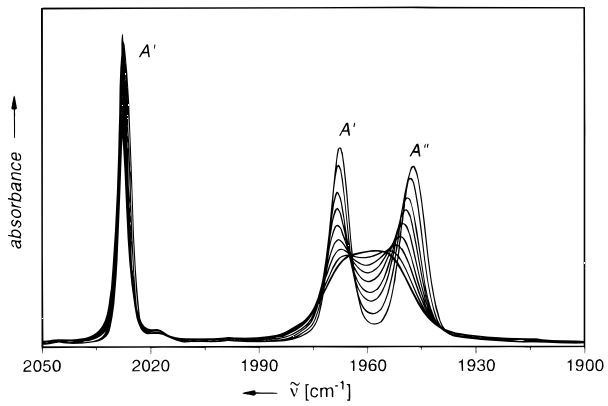

Figure 4. The ν(CO) bands in the variable-temperature IR spectra of Fe(CO)$_3$(η^4-1,5-cod) (**1**), recorded in 2-methylpentane solution at 293 K (bold line) and 273/253/233/213/193/173/153/133 K.

Table 2. The CO Stretching Vibrational Bands in the IR Spectra of Fe(CO)$_3$(η^4-1,5-cod) (**1**), Fe(CO)$_3$(η^4-1,3-butadiene) (**4**), and Fe(CO)(η^4-1,3-butadiene)$_2$ (**5**), Recorded in 2-Methylpentane Solution and Analyzed by Curve Fitting[25] to the Voigt Function

complex	T [K]	$\tilde{\nu}_{max}$ [cm^{-1}]	assignment	rel intensity [%]	$\Gamma^{(L)}$ [a] [cm^{-1}]	$\Gamma^{(G)}$ [a] [cm^{-1}]
1	133	2026.9	A'	27.3	1.33	2.77
		1967.7	A'	34.6	2.82	4.51
		1947.4	A''	38.2	2.37	6.69
4	133	2055.2	A'	22.3	1.58	1.70
		1987.8	A'	42.0	1.53	3.76
		1977.3	A''	35.8	2.07	3.81
4	293	2056.1	A'	22.5	2.87	1.13
		1990.3	A'	43.8	3.76	0.98
		1980.1	A''	33.7	3.83	1.20
5	133	1983.5			1.78	6.34
5	293	1985.9			5.47	2.75

[a] Lorentzian and Gaussian line width components.

conditions where the kinetic effects of the CO site exchange should be of minor importance, although not entirely negligible (vide infra). Fitting[25] to the Voigt function, commonly applicable to IR absorptions in liquid-phase systems,[26] gave satisfactory results indicating that all three band shapes are predominantly Gaussian in character (Table 2).

For comparison, the variable-temperature IR spectra of the 1,3-butadiene complex **4**[27] were recorded in the same solvent. As expected, and previously noted,[1,2,4] no spectacular changes in the band profiles occur upon raising the temperature from 133 to 293 K (Figure 5), since this complex is known to be fluxional on the NMR time scale and thus appears rigid on the vibrational time scale. The activation barrier for the CO site exchange amounts to ca. 9 kcal mol^{-1}, as previously determined by means of variable-temperature ^{13}C NMR spectroscopy[28] and recently confirmed by calculations with density functional theory methods.[19]

However, there are some subtle temperature effects which must not be ignored. First of all, we note that upon raising the temperature the positions of all band maxima are shifted to higher frequencies, but less pronounced in the high-frequency,

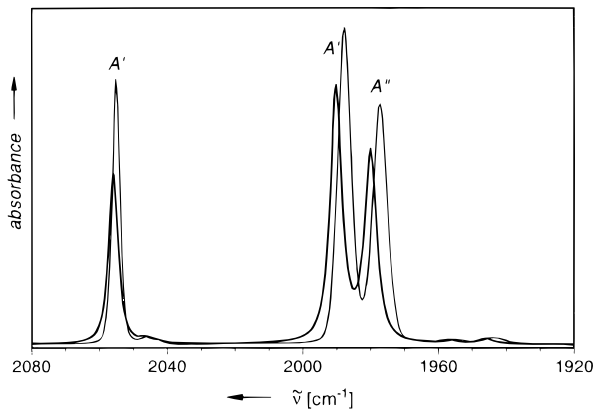

Figure 5. The ν(CO) bands in the IR spectrum of Fe(CO)$_3$(η^4-1,3-butadiene) (**4**) recorded in 2-methylpentane solution at 293 K (bold line) and 133 K.

in-phase A' ν(CO) mode, compared with the two out-of-phase modes (A' and A'') at lower frequencies (Table 2). Moreover, examination of the band contours by means of curve fitting[25] reveals additional significant changes with temperature. Fitting to the Voigt function gave satisfactory results over the entire range of temperatures. Again, the band profiles in the low-temperature spectrum are found to be predominantly Gaussian in character, whereas at ambient temperature the Lorentzian component prevails, i.e., the Gaussian and Lorentzian line width parameters $\Gamma^{(G)}$ and $\Gamma^{(L)}$ exhibit opposite changes with temperature (Table 2). Concerning the relative intensities of the three ν(CO) bands, there is apparently no change with temperature, but the total integrated intensity gradually decreases by a factor of ca. 2% upon raising the temperature in steps of 20 K. This latter effect is not surprising as it seems to reflect a temperature-dependent decrease in solution density. Similar observations were made with a variety of other metal carbonyls including, e.g., the monocarbonyl complex Fe(CO)(η^4-1,3-butadiene)$_2$ (**5**)[27,29] (Table 2). The single ν(CO) mode of **5** shows the same temperature-dependent trends as **4** with regard to both the frequency shift and the changes in the Lorentzian and Gaussian line width parameters.

These effects probably arise from temperature-dependent solute−solvent interactions and from the dynamics of vibrational relaxation and other processes relevant to the band positions and to the homogeneous and inhomogeneous contributions to the line widths. As recently shown for the T_{1u} ν(CO) mode of W(CO)$_6$,[30] picosecond IR photon echo and pump−probe experiments could provide for a better understanding of these phenomena, but such information is not yet available for the compounds investigated in the present study. Thus, we have no choice but to take the observed trends into account in an empirical fashion.

Infrared Band Shapes and Chemical Exchange. As mentioned in the Introduction, the dynamic effects of very fast reversible reactions and rearrangements on Raman[8,11−13] and infrared[9,10,13,16,17,20] band shapes have been discussed in the literature. In most cases, the quantitative description is based on the solutions to a set of Bloch equations modified for chemical exchange and thus parallels the treatment of chemical exchange in nuclear magnetic resonance.[14,31−33]

(25) Curve fitting was performed with the appropriate options of the GRAMS/32 (V4.0) software package; Galactic Industries Corporation, 395 Main Street, Salem, NH 03079.

(26) Jansson, P. A. *Deconvolution with Applications in Spectroscopy*; Academic Press: San Diego, 1984.

(27) Koerner von Gustorf, E.; Pfajfer, Z.; Grevels, F.-W. *Z. Naturforsch. B* **1971**, *26*, 66−67. The previously reported preparation of **4** was modified by using *n*-pentane as the solvent instead of benzene.

(28) (a) Kruczynski, L.; Takats, J. *J. Am. Chem. Soc.* **1974**, *96*, 932−934. (b) Kruczynski, L.; Takats, J. *Inorg. Chem.* **1976**, *15*, 3140−3147.

(29) Koerner von Gustorf, E.; Buchkremer, J.; Pfajfer, Z.; Grevels, F.-W. *Angew. Chem.* **1971**, *83*, 249−250; *Angew. Chem., Int. Ed. Engl.* **1971**, *10*, 260−261.

(30) Tokmakoff, A.; Fayer, M. D. *J. Phys. Chem.* **1995**, *103*, 2810−2826.

(31) McConnell, H. M. *J. Chem. Phys.* **1958**, *28*, 430−431.

(32) Sack, R. A. *Mol. Phys.* **1958**, *1*, 163−167.

An adaptation of Gordon's work[34] on the Fourier transform relationship between the infrared band shape and the correlation function for the dipole moment of the molecule will be used here to generalize the Bloch description of vibrational exchange in a straightforward manner. The infrared absorption $I(\omega)$, at frequency $\omega = 2\pi\nu = 2\pi\tilde{\nu}c_0$ (in s^{-1}), can be expressed[34] as a Fourier transform

$$I(\omega) = \mathrm{Re}\left\{\int_0^\infty G(t)\exp(-i\omega t)\,\mathrm{d}t\right\} \tag{1}$$

of the time correlation function $G(t)$ for the dipole moment μ of the vibrating molecule

$$G(t) = \sum_{i,f}\rho_i\langle i\,|\mu(0)|\,f\rangle\,\langle f|\mu(t)|i\rangle \tag{2}$$

where $|i\rangle$ and $|f\rangle$ are the initial and final vibrational states of the molecule involved in the absorption process, ρ_i is the population of state $|i\rangle$, and $\mu(t)$ is the Heisenberg operator, $\exp(iHt/\hbar)\mu\cdot\exp(-iHt/\hbar)$. If one ignores the effects of rotational motion (i.e., one assumes that the vibrational correlation function contains a Lorentzian line width component which includes the rotational contribution to the bandwidth), expands μ in terms of the normal coordinates $\{Q_\alpha\}$ of the molecule, and assumes that different vibrational modes are uncorrelated, the vibrational correlation function can be written as

$$G_{\mathrm{vib}}(t) = \sum_\alpha\sum_{i,f}\rho_i\left(\frac{\partial\mu}{\partial Q_\alpha}\right)^2\langle i|Q_\alpha(0)|f\rangle\,\langle f|Q_\alpha(t)|i\rangle \tag{3}$$

Since we are interested in the fundamental CO stretching bands of the organometal carbonyl complexes, the only state $|i\rangle$ of importance is the one in which all CO stretching modes are in their lowest vibrational states, which we designate $|0\rangle$. Provided that the vibrations are harmonic, the only excited vibrational state $|f\rangle$ for which the transition dipole integral $\langle 0|Q_\alpha(0)|f\rangle$ is nonzero is that state, which we denote $|1_\alpha\rangle$, in which the mode Q_α is in its first excited state. Hence

$$G_{\mathrm{vib}}(t) = \sum_\alpha P_\alpha D_\alpha(0)D_\alpha(t) \tag{4}$$

where

$$P_\alpha = \rho_0\left(\frac{\partial\mu}{\partial Q_\alpha}\right)^2 \tag{5}$$

and

$$D_\alpha(t) = \langle 1_\alpha|Q_\alpha(t)|0\rangle \tag{6}$$

represent an intensity factor and the transition dipole moment, respectively, of normal mode α and[35]

$$D_\alpha(0) = (2\omega_\alpha/\hbar)^{-1/2} \tag{7}$$

where ρ_0 is the population of state $|0\rangle$ and ω_α the frequency of the mode.

In accordance with the results of the ν(CO) band profile analyses, the infrared spectrum will be treated as a superposition of Voigt line shapes centered at the vibrational frequencies ω_α.

(33) (a) Johnson, C. S., Jr. *Adv. Magn. Reson.* **1965**, *1*, 33−102. (b) Kaplan, J. I. *J. Chem. Phys.* **1958**, *28*, 278−282. (c) Kaplan, J. I. *J. Chem. Phys.* **1958**, *29*, 462.

(34) (a) Gordon, R. G. *J. Chem. Phys.* **1965**, *43*, 1307−1312. (b) Gordon, R. G. *J. Chem. Phys.* **1965**, *43*, 2587−2594. (c) Gordon, R. G. *Adv. Magn. Reson.* **1968**, *3*, 1−42.

This implies that, in the absence of chemical exchange, $D_\alpha(t)$ follows the equation of motion

$$\frac{\mathrm{d}D_\alpha}{\mathrm{d}t} = \{i\omega_\alpha - \Gamma_\alpha^{(\mathrm{L})} - t[\Gamma_\alpha^{(\mathrm{G})}]^{-2}\}D_\alpha \tag{8}$$

where the term $-\Gamma_\alpha^{(\mathrm{L})}D_\alpha$ accounts for vibrational relaxation and rotational effects which give rise to Lorentz broadening of the band, and the term $-t[\Gamma_\alpha^{(\mathrm{G})}]^{-2}D_\alpha$ represents the effects responsible for Gaussian contributions to the line shape. At time t, the transition moment is given by

$$D_\alpha(t) = D_\alpha(0)\exp\left[(i\omega_\alpha - \Gamma_\alpha^{(\mathrm{L})})t - \frac{t^2}{2}[\Gamma_\alpha^{(\mathrm{G})}]^{-2}\right] \tag{9}$$

and the vibrational correlation function is given by

$$G_{\mathrm{vib}}(t) = \frac{2}{\hbar}\sum_\alpha(P_\alpha/\omega_\alpha)\exp\left[(i\omega_\alpha - \Gamma_\alpha^{(\mathrm{L})})t - \frac{t^2}{2}[\Gamma_\alpha^{(\mathrm{G})}]^{-2}\right] \tag{10}$$

If we drop the factor $2/\hbar$, we find that the infrared spectral profile, in the absence of chemical exchange, is

$$I(\omega) = \sum_\alpha(P_\alpha/\omega_\alpha)V(\omega_\alpha,\Gamma_\alpha^{(\mathrm{L})},\Gamma_\alpha^{(\mathrm{G})}) \tag{11}$$

where

$$V(\omega_\alpha,\Gamma_\alpha^{(\mathrm{L})},\Gamma_\alpha^{(\mathrm{G})}) = \int_0^\infty\exp\left[(i\omega_\alpha - \Gamma_\alpha^{(\mathrm{L})})t - \frac{t^2}{2}[\Gamma_\alpha^{(\mathrm{G})}]^{-2}\right]\exp(-i\omega t)\,\mathrm{d}t \tag{12}$$

is a normalized Voigt line shape centered at frequency ω_α and characterized by a Lorentzian width parameter $\Gamma_\alpha^{(\mathrm{L})}$ and a Gaussian width parameter $\Gamma_\alpha^{(\mathrm{G})}$.

Dynamic effects arising from very fast reversible reactions will be accounted for by an exchange term

$$\left(\frac{\mathrm{d}D_\alpha}{\mathrm{d}t}\right)_{\text{chemical exchange}} = \sum_{\alpha'}K_{\alpha\alpha'}D_{\alpha'} \tag{13}$$

where $K_{\alpha\alpha'}$ are the elements of the exchange matrix **K** describing the rates at which the vibrational dipole moments of the different modes are interchanged by the chemical exchange process. Following the standard "modified Bloch equation" approach,[31−33] we assume that this term can be added to the equation of motion for the transition dipole moment, eq 8, thus yielding

$$\frac{\mathrm{d}D_\alpha}{\mathrm{d}t} = \{i\omega_\alpha - \Gamma_\alpha^{(\mathrm{L})} - t[\Gamma_\alpha^{(\mathrm{G})}]^{-2}\}D_\alpha + \sum_{\alpha'}K_{\alpha\alpha'}D_{\alpha'} \tag{14}$$

This set of coupled differential equations must be solved to determine the infrared spectral profile for the situation where exchange is operative. We shall first determine the exact solutions to eq 14 for the case that the Gaussian broadening terms $t[\Gamma_\alpha^{(\mathrm{G})}]^{-2}D_\alpha$ are negligible and thus taken to be zero, and then derive an approximate solution for the set of equations including these terms.

Ignoring the Gaussian broadening terms, one may write eq 14 in the matrix form

$$\mathrm{d}\mathbf{D}/\mathrm{d}t = -\mathbf{A}\cdot\mathbf{D} \tag{15}$$

where **D** is a column vector with elements $D_\alpha(t)$, and the matrix **A** has the elements

$$A_{\alpha\alpha'} = \begin{cases} -i\omega_\alpha + \Gamma_\alpha^{(L)} - K_{\alpha\alpha} & \text{for } \alpha = \alpha' \\ -K_{\alpha\alpha'} & \text{for } \alpha \neq \alpha' \end{cases} \quad (16)$$

The solution to eq 15 is

$$D_\alpha(t) = \sum_j \exp(-\Lambda_j t) S_{\alpha j} \sum_{\alpha'} S^{-1}_{j\alpha'} D_{\alpha'}(0) \quad (17)$$

where **S** (with elements $S_{\alpha j}$) is the matrix of eigenvectors of **A**, $\mathbf{S}^{-1}$ (with elements $S^{-1}_{j\alpha'}$) is the inverse of **S**, and Λ (with elements Λ_j) is a diagonal matrix containing the corresponding eigenvalues of **A**. Since the frequencies of the CO stretching vibrational modes span a narrow range (2040−1920 cm^{-1}), such that $D_\alpha(0)$ does not vary strongly with α, it is convenient to replace eq 7 by the approximation

$$D_\alpha(0) \cong (2\omega_{\text{average}}/\hbar)^{-1/2} \quad (18)$$

where ω_{average} is the average CO stretching vibrational frequency. With this approximation, we can write the vibrational correlation function as

$$G_{\text{vib}}(t) = \sum_{\alpha,\alpha',j} D_\alpha(0)\rho_0 S_{\alpha j} \exp(-\Lambda_j t) S^{-1}_{j\alpha'} D_{\alpha'}(0)$$
$$= \vec{\mathbf{p}}^{\dagger}\cdot\mathbf{S}\cdot\exp(-\Lambda t)\cdot\mathbf{S}^{-1}\cdot\vec{\mathbf{1}} \quad (19)$$

where $\vec{\mathbf{p}}$ is a column vector whose elements

$$p_\alpha = \rho_0\left(\frac{\partial\mu}{\partial Q_\alpha}\right)^2 (2\omega_{\text{average}}/\hbar) \quad (20)$$

are proportional to the intensities of the vibrational transitions in the absence of exchange, and $\vec{\mathbf{1}}$ is a column vector with all elements equal to 1. The infrared spectral profile in the presence of vibrational exchange, but with no Gaussian line broadening, is given by

$$I(\omega) = \text{Re}\{\vec{\mathbf{p}}^{\dagger}\cdot\mathbf{S}\cdot(\Lambda + \omega\mathbf{1})^{-1}\cdot\mathbf{S}^{-1}\cdot\vec{\mathbf{1}}\} \quad (21)$$

The spectrum therefore consists of a set of Lorentzian type bands, centered at frequencies $-\text{Im}\{\Lambda_j\}$, with line widths $\text{Re}\{\Lambda_j\}$ and intensities $\sum_{\alpha,\alpha'} p_\alpha S_{\alpha j} S_{j\alpha'}{}^{-1}$. Equation 21 is a generalization of the results previously obtained for the two-site exchange case with the density matrix formalism.[16] It is identical in form to that obtained by Sack[32] in his treatment of the effects of chemical exchange on nuclear magnetic resonance spectra.

When Gaussian line broadening cannot be neglected, the above treatment must be modified. Equation 15, the matrix form of eq 14 without the Gaussian term, is replaced by

$$\frac{d\mathbf{D}}{dt} = -(\mathbf{A} + t\mathbf{G})\cdot\mathbf{D} \quad (22)$$

where **G** is a diagonal matrix with the elements

$$G_{\alpha\alpha} = [\Gamma_\alpha^{(G)}]^{-2} \quad (23)$$

If we neglect the off-diagonal elements of the matrix $\mathbf{S}^{-1}\cdot\mathbf{G}\cdot\mathbf{S}$, eq 22 can be shown to have the approximate solution

$$D_\alpha(t) = \sum_j \exp\left[-\Lambda_j t - \frac{G'_j t^2}{2}\right] S_{\alpha j} \sum_{\alpha'} S^{-1}_{j\alpha'} D_{\alpha'}(0) \quad (24)$$

where

$$G'_j = [\mathbf{S}^{-1}\cdot\mathbf{G}\cdot\mathbf{S}]_{jj} \quad (25)$$

The only difference between eq 17, obtained by neglecting Gaussian broadening, and eq 24 is the presence of the term $-G'_j t^2/2$ in the exponential function of the latter equation. Having included Gaussian broadening in this approximate fashion, one obtains the vibrational correlation function

$$G_{\text{vib}}(t) = \vec{\mathbf{p}}^{\dagger}\cdot\mathbf{S}\cdot\exp(-\Lambda t - \mathbf{G}' t^2/2)\cdot\mathbf{S}^{-1}\cdot\vec{\mathbf{1}} \quad (26)$$

The infrared spectral profile is given by

$$I(\omega) = \text{Re}\{\sum_j V(-\text{Im}\{\Lambda_j\}, \text{Re}\{\Lambda_j\}, [G'_j]^{-1/2}) \sum_{\alpha,\alpha'} p_\alpha S_{\alpha j} S^{-1}_{j\alpha'}\} \quad (27)$$

where $V(-\text{Im}\{\Lambda_j\}, \text{Re}\{\Lambda_j\}, [G'_j]^{-1/2})$ is a normalized Voigt function centered at frequency $-\text{Im}\{\Lambda_j\}$, with Lorentzian width $\text{Re}\{\Lambda_j\}$, Gaussian width $[G'_j]^{-1/2}$, and intensity $\sum_{\alpha,\alpha'} p_\alpha S_{\alpha j} S_{j\alpha'}{}^{-1}$.

The Rate of Transition Dipole Moment Transfer between Vibrational Modes. The results presented above are generalizations of earlier work dealing with the evaluation of picosecond kinetic data from exchange-broadened vibrational band profiles.[8−13,16,20] As a common feature, the systems investigated in those studies were treated in terms of a model oscillator existing in two different, rapidly interconverting forms or environments, A and B,[36] with different vibrational frequencies ω_a and ω_b, Scheme 5. The dynamics of the transition dipole moment exchange between the two modes could thus be equated with the kinetics of the underlying process. No other, specific information on the normal modes was needed, and Lorentzian-type band shapes were implicitly presumed.

Scheme 5

$$\underset{\omega_a}{\text{A}} \underset{k_b}{\overset{k_a}{\rightleftharpoons}} \underset{\omega_b}{\text{B}}$$

An approach at such a rudimentary level would clearly not give an adequate description of the CO site exchange in $Fe(CO)_3(\eta^4\text{-}1,5\text{-cod})$ (**1**) and related compounds mentioned in the Introduction. Here we are dealing with a degenerate process, Scheme 6, and the spectral changes with temperature (Figure 4) accordingly involve different modes of one and the same molecule. The rates of transition dipole moment transfer between these modes were introduced above in a purely phenomenological fashion, eq 13, which requires further amplification and justification.

In the energy-factored CO force field approximation,[22] the CO stretching modes of metal carbonyls are characterized by normal coordinates $\{Q_\alpha\}$ which are linear combinations of the individual CO displacement coordinates $\{r_i\}$. In an $M(CO)_3L$

(35) Wilson, E. B., Jr.; Decius, J. C.; Cross, P. C. *Molecular Vibrations*; McGraw-Hill: New York, 1955.

(36) An extension to more complicated reaction systems of the type **A** ⇌ **B** ⇌ **C**, as outlined by Strehlow et al.,[11,12] still involves only one vibrational mode for each of the various species.

Scheme 6

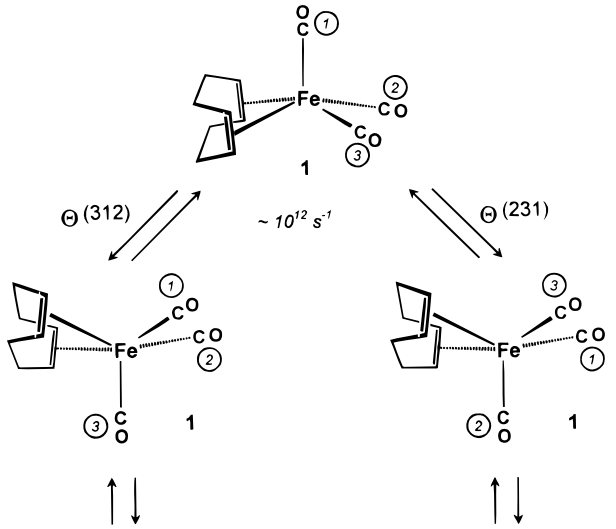

complex, such as $Fe(CO)_3(\eta^4$-diene), there are three ν(CO) normal coordinates Q_1, Q_2, and Q_3, as listed in Table 1 for the case of the 1,5-cod complex **1**. The relationship between the normal coordinates $\{Q_\alpha\}$ and the CO displacement coordinates $\{r_i\}$ may be written in matrix form as

$$\mathbf{Q} = \mathbf{N}\cdot\mathbf{r} \tag{28}$$

where **Q** is a column vector with elements Q_1, Q_2, and Q_3, **r** is a column vector with elements r_1, r_2, and r_3, and **N** is a matrix with elements $N_{\alpha i}$, which defines the linear combinations.[37]

In the event of a rearrangement, Scheme 6, the CO ligands interchange their positions and the coordinates **Q** are transformed into $\tilde{\mathbf{Q}}$ according to

$$\tilde{\mathbf{Q}} = \mathbf{N}\cdot\Theta\cdot\mathbf{r} \tag{29}$$

where Θ is the matrix describing the permutation of the displacement coordinates r_1, r_2, and r_3 during the event. Since

$$\mathbf{r} = \mathbf{N}^\dagger\cdot\mathbf{Q} \tag{30}$$

where $\mathbf{N}^\dagger$ is the transpose of matrix **N**, the normal mode coordinates after exchange are given by

$$\tilde{\mathbf{Q}} = \mathbf{N}\cdot\Theta\cdot\mathbf{N}^\dagger\cdot\mathbf{Q} \tag{31}$$

The transition moments $D_\alpha = \langle 1_\alpha|Q_\alpha(t)|0\rangle$ are transformed during the exchange process, since they depend on the normal coordinates Q_α. Note that, in addition to Q_α being transformed into $\tilde{Q}_\alpha$ by exchange, the wave function $|1_\alpha\rangle$ will be transformed into $|\tilde{1}_\alpha\rangle$, because it is a function of coordinate Q_α, while the ground-state wave function $|0\rangle$ remains unchanged, as shown below.

Following Wilson, Decius, and Cross,[35] the ground and singly excited vibrational wave functions are

$$|0\rangle = \prod_{\alpha=1}^{n} N_\alpha \cdot \exp\left[-\frac{1}{2}\sum_{\alpha=1}^{n}(\gamma_\alpha Q_\alpha^2)\right] \tag{32}$$

(37) Matrix **N** and the commonly used matrix **L**[35] differ by a constant factor, the square root of the reduced mass of the CO unit, as these matrixes have the properties $\mathbf{N}\cdot\mathbf{N}^\dagger = \mathbf{1}$ and $\mathbf{L}\cdot\mathbf{L}^\dagger = \mathbf{G}$: Bor, G. *Inorg. Chim. Acta* **1967**, *1*, 81−92.

and

$$|1_\alpha\rangle = Q_\alpha\sqrt{2\gamma_\alpha}|0\rangle \tag{33}$$

where

$$N_\alpha = (\gamma_\alpha/\pi)^{1/4} \tag{34}$$

and

$$\gamma_\alpha = \frac{\omega_\alpha}{\hbar} \tag{35}$$

With the approximation $\omega_\alpha \cong \omega_{\text{average}}$ (vide supra) and, accordingly,

$$\gamma_\alpha \cong \gamma = \frac{\omega_{\text{average}}}{\hbar} \tag{36}$$

the vibrational wave functions can be written as

$$|0\rangle \cong \prod_{\alpha=1}^{n} N_\alpha \cdot \exp\left[-\frac{\gamma}{2}\sum_{\alpha=1}^{n} Q_\alpha^2\right] \tag{37}$$

and

$$|1_\alpha\rangle \cong Q_\alpha\sqrt{2\gamma}|0\rangle \tag{38}$$

As mentioned above, both $Q_\alpha(t)$ and $|1_\alpha\rangle$ will be transformed in the event of a CO site exchange, whereas $|0\rangle$ is not affected because $\Theta^{-1} = \Theta^\dagger$ and $\sum_\alpha(\tilde{Q}_\alpha)^2 = \sum_{\alpha'}(Q_{\alpha'})^2$. The transition moment after exchange will thus be given by

$$\tilde{D}_\alpha(t) = \langle\tilde{1}_\alpha|\tilde{Q}_\alpha(t)|0\rangle$$

$$\tilde{D}_\alpha(t) \cong \sum_{i,j,\alpha'} N_{\alpha i}\Theta_{ij}N_{j\alpha'}^\dagger\langle 1_{\alpha'}|\sum_{\tilde{\imath},\tilde{\jmath},\tilde{\alpha}'} N_{\alpha\tilde{\imath}}\Theta_{\tilde{\imath}\tilde{\jmath}}N_{\tilde{\jmath}\tilde{\alpha}'}^\dagger Q_{\tilde{\alpha}'}(t)|0\rangle$$

$$\tilde{D}_\alpha(t) \cong \sum_{\alpha'} Z_{\alpha\alpha'}D_{\alpha'} \tag{39}$$

where

$$Z_{\alpha\alpha'} = (\sum_{i,j} N_{\alpha i}\Theta_{ij}N_{j\alpha'}^\dagger)^2 \tag{40}$$

are the elements of matrix **Z**, which describes the transformation of the vibrational dipole moments during the event of CO site exchange.

In the density matrix treatment of chemical exchange effects in nuclear magnetic resonance,[33] the rate of change of the density matrix during exchange is taken to be

$$\left(\frac{\mathrm{d}\rho}{\mathrm{d}t}\right)_{\text{chemical exchange}} = k_{\text{react}}(\tilde{\rho} - \rho) \tag{41}$$

where $\tilde{\rho}$ is the density matrix after an exchange event, and k_{react} is the (first-order) rate constant for the underlying chemical reaction. Following this approach, we shall assume that the effect of exchange on the vibrational dipole moment can be expressed as

$$\left(\frac{\mathrm{d}D_\alpha}{\mathrm{d}t}\right)_{\text{chemical exchange}} = k_{\text{react}}(\tilde{D}_\alpha - D_\alpha) \tag{42}$$

which is equivalent to eq 13 in the previous section. In matrix form eq 42 reads as

$$\left(\frac{d\mathbf{D}}{dt}\right)_{\text{chemical exchange}} = \mathbf{K}\cdot\mathbf{D} \tag{43}$$

where $\mathbf{K} = k_{\text{react}}(\mathbf{Z} - \mathbf{1})$, such that the elements of matrix **K** are

$$K_{\alpha\alpha'} = k_{\text{react}}(Z_{\alpha\alpha'} - \delta_{\alpha\alpha'}) \tag{44}$$

If the exchange process involves *n* equiprobable permutations characterized by the permutation matrices $\Theta^{(1)}$, $\Theta^{(2)}$, ..., $\Theta^{(n)}$, the matrix **K** will have the elements

$$K_{\alpha\alpha'} = \frac{k_{\text{react}}}{n}\sum_{l=1}^{n}(Z^{(l)}_{\alpha\alpha'} - \delta_{\alpha\alpha'}) \tag{45}$$

where

$$Z^{(l)}_{\alpha\alpha'} = (\sum_{i,j} N_{\alpha i}\Theta^{(l)}_{ij}N^{\dagger}_{j\alpha'})^2 \tag{46}$$

In the case of **1** we have to consider two equiprobable permutations of the CO displacement coordinates r_i, involving either a clockwise or an anticlockwise turnstile rotation, as illustrated in Scheme 6. The two processes are characterized by the permutation matrixes

$$\Theta^{(231)} = \begin{pmatrix}0&1&0\\0&0&1\\1&0&0\end{pmatrix} \text{ and } \Theta^{(312)} = \begin{pmatrix}0&0&1\\1&0&0\\0&1&0\end{pmatrix}$$

i.e., the first one takes CO(2) and the second one takes CO(3) into the apical position initially occupied by CO(1). The *ν*-(CO) normal coordinates of complex **1** are listed in Table 1. With $\Theta^{(231)}$,

$$\mathbf{N} = \begin{pmatrix}0.6659&0.5275&0.5275\\0.7461&-0.4708&-0.4708\\0&0.7071&-0.7071\end{pmatrix}$$

and

$$\mathbf{N}^{\dagger} = \begin{pmatrix}0.6659&0.7461&0\\0.5275&-0.4708&0.7071\\0.5275&-0.4708&-0.7071\end{pmatrix}$$

eq 46 yields the elements $Z^{(231)}_{\alpha\alpha'}$ of the matrix

$$\mathbf{Z}^{(231)} = \begin{pmatrix}0.9622&0.0283&0.0096\\0.0283&0.2313&0.7405\\0.0096&0.7405&0.2500\end{pmatrix}$$

which describes the transformation of the vibrational dipole moments during the CO site exchange event illustrated on the right-hand side of Scheme 6. Due to the C_s symmetry of complex **1**, the same numerical result is obtained with $\Theta^{(312)}$ (which characterizes the exchange event on the left-hand side of Scheme 6), i.e., $\mathbf{Z}^{(312)} = \mathbf{Z}^{(231)} = \mathbf{Z}$. Hence it follows that eq 45 takes the simpler form of eq 44, i.e., the kinetics of

Scheme 7

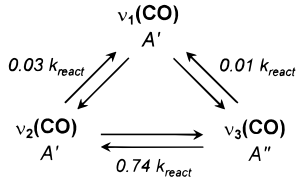

vibrational dipole moment interchange between the three *ν*(CO) modes of the complex is described by the matrix

$$\mathbf{K} = k_{\text{react}}(\mathbf{Z} - \mathbf{1}) = k_{\text{react}}\begin{pmatrix}-0.0378&0.0283&0.0096\\0.0283&-0.7687&0.7405\\0.0096&0.7405&-0.7500\end{pmatrix} \tag{47}$$

This result, visualized in Scheme 7, immediately rationalizes the observation that the low-frequency pair of bands, ν_2(CO) (*A*′) and ν_3(CO) (*A*″), in the variable-temperature IR spectra of complex **1** (Figure 4) is much more affected by exchange than the ν_1(CO) (*A*′) band at higher frequency. The rate constant for the interchange of dipole moment between ν_2(CO) (*A*′) and ν_3(CO) (*A*″) is much higher, by a factor of 25, compared with the respective rate constants for the interchange of dipole moment between ν_1(CO) (*A*′) and either of the other two modes, the sum of which does not exceed 4% of the rate constant of the underlying CO site exchange process.

The Low Barrier of CO Site Exchange in Fe(CO)₃(η⁴-1,5-cod) (1) Evaluated by *ν*(CO) IR Band Shape Simulation. The variable-temperature *ν*(CO) IR spectra of **1** (Figure 4) were simulated on the basis of eq 27 with trial values of the rate constant k_{react} for the CO site exchange process, using the exchange matrix **K** determined from eq 47. The spectral parameters in the absence of exchange (frequencies $\omega_\alpha = 2\pi\tilde{\nu}_\alpha c_0$; line width components $\Gamma^{(L)}_\alpha$ and $\Gamma^{(G)}_\alpha$; intensity factors p_α), required as input data in the simulation, were adapted from the spectrum recorded at 133 K (Table 2), but with temperature-dependent modifications according to the trends recognized from the variable-temperature spectra of Fe(CO)₃(η⁴-1,3-butadiene) (**4**) and Fe(CO)(η⁴-1,3-butadiene)₂ (**5**) (vide supra, Table 2).

Careful examination of the solution spectra displayed in Figure 4 reveals that even at 133 K the CO site exchange is not entirely arrested, since the continuously increasing separation of the ν_2(CO) (*A*′) and ν_3(CO) (*A*″) band maxima has not yet reached a constant value. Thus, instead of using $\Delta\tilde{\nu} = 20.3$ cm^{-1} (Table 2) observed in the solution spectrum at 133 K, we adopt the value of $\Delta\tilde{\nu} = 20.7$ cm^{-1} from the low-temperature matrix spectrum at 10 K (Table 1), to obtain a reasonable estimate of the frequency input data (2026.9, 1967.9, and 1947.2 cm^{-1}) for the simulation of the spectrum in 2-methylpentane at 133 K. With $k_{\text{react}} = 1.5 \times 10^{11}$ s^{-1} and modified values for the Lorentzian and Gaussian width components (see Table 3), the experimental spectrum could be satisfactorily reproduced.

For the simulation of the spectra of **1** at higher temperatures the input frequency data were modified, in steps of +20 K (Table 3), by adding +0.1 cm^{-1} to the ν_1(CO) (*A*′) frequency and +0.3 cm^{-1} to the ν_2(CO) (*A*′) and ν_3(CO) (*A*″) frequencies, thereby adopting the temperature dependence of the respective bands in the spectra of the 1,3-butadiene complex **4** (Figure 5, Table 2). With these frequency data, an approximate reproduction of the experimental spectra was attained by using rate constants which were varied from 2.5×10^{11} s^{-1} at 155 K to 1.54×10^{12} s^{-1} at 293 K (Table 3). For further refinement of the simulations, the Gaussian and Lorentzian line width input

Table 3. Rate Constants of CO Site Exchange and Spectral Parameters Used as Input Data in the Simulation of the Variable-Temperature ν(CO) IR Spectra of $Fe(CO)_3(\eta^4$-1,5-cod) (**1**)[41]

T [K]	k_{react} [s^{-1}]	$\tilde{\nu}_{max}$ [cm^{-1}]	$\Gamma^{(L)}$ [cm^{-1}]	$\Gamma^{(G)}$ [cm^{-1}]
133	1.5×10^{11}	2026.9	1.1	2.9
		1967.9	1.1	4.8
		1947.2	0.9	6.8
153	2.5×10^{11}	2027.0	1.2	2.4
		1968.2	1.5	4.3
		1947.6	1.4	6.1
173	4.3×10^{11}	2027.1	1.7	1.5
		1968.5	2.0	3.2
		1947.9	2.0	5.0
193	5.6×10^{11}	2027.2	1.8	1.2
		1968.8	2.1	2.8
		1948.3	2.1	4.6
213	7.2×10^{11}	2027.3	1.9	1.0
		1969.1	2.6	2.0
		1948.6	2.7	4.0
233	8.6×10^{11}	2027.4	2.0	0.9
		1969.4	3.8	1.7
		1948.9	4.3	2.1
253	1.05×10^{12}	2027.5	2.2	0.9
		1967.7	4.2	1.6
		1949.2	4.7	1.5
273	1.27×10^{12}	2027.6	2.4	0.7
		1970.0	5.3	1.1
		1949.5	5.4	0.8
293	1.54×10^{12}	2027.6	2.6	0.7
		1970.3	5.6	0.9
		1949.8	5.6	1.2

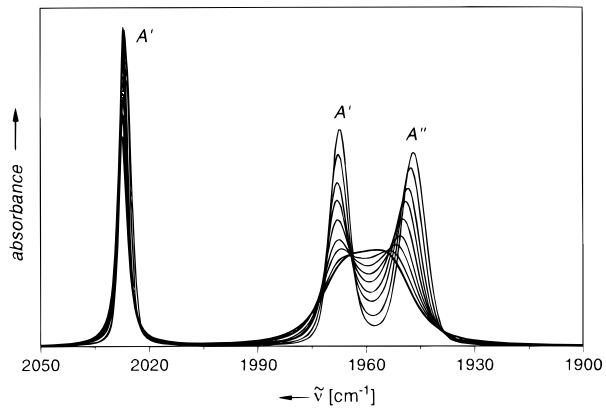

Figure 6. Simulation of the ν(CO) bands in the variable-temperature IR spectra of $Fe(CO)_3(\eta^4$-1,5-cod) (**1**), using rate constants for the CO site exchange process ranging from 1.5×10^{11} s^{-1} at 133 K to 1.54×10^{12} s^{-1} at 293 K (bold line) and spectral parameters listed in Table 3.[41]

parameters, $\Gamma^{(G)}$ and $\Gamma^{(L)}$, were varied toward smaller values for the former and higher values for the latter (see Table 3) until the best fitting to the experimental spectral profiles was achieved at each temperature. The final results of the simulations are collectively displayed in Figure 6 for comparison with the variable-temperature spectra in Figure 4, illustrating an excellent agreement. Note that the minor features in the experimental spectra (Figure 4) near 2020 cm^{-1}, which represent ^{13}CO satellite absorptions, are of course not reproduced in the simulations.

Both the Eyring plot of ln(k/T) vs 1/T (Figure 7) and the Arrhenius plot of ln(k) vs 1/T give fairly straight lines, the slopes of which yield $\Delta H^{\ddagger} = 0.7$ kcal·mol^{-1} and $E_a = 1.1$ kcal·mol^{-1}, respectively. This activation barrier for the CO site exchange in the η^4-1,5-cod complex **1** is in excellent agreement with the value of 0.5 kcal·mol^{-1} (0.6 kcal·mol^{-1} without zero-point

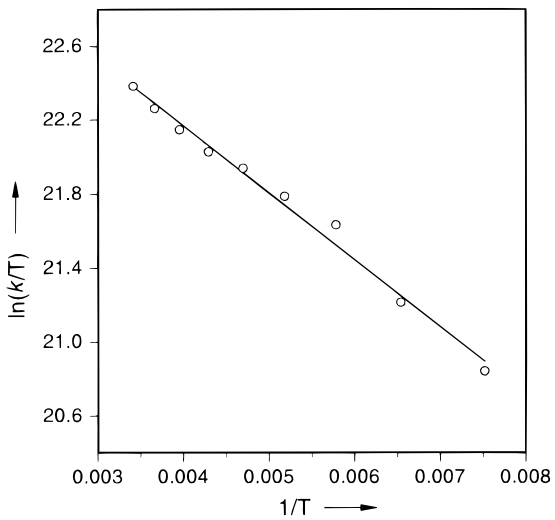

Figure 7. Eyring plot of ln(k/T) vs 1/T yielding $\Delta H^{\ddagger} = 0.7$ kcal·mol^{-1} and $\Delta S^{\ddagger} = -0.3$ cal·K^{-1}·mol^{-1} for the CO site exchange process in $Fe(CO)_3(\eta^4$-1,5-cod) (**1**).

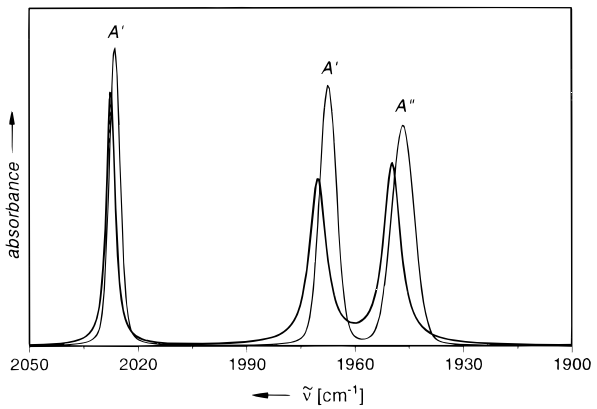

Figure 8. The hypothetical IR ν(CO) pattern of $Fe(CO)_3(\eta^4$-1,5-cod) (**1**) in the absence of CO site exchange at 293 K (bold line) and 133 K simulated with the respective spectral parameters listed in Table 3,[41] but with $k_{react} = 0$ s^{-1}.

energy correction) calculated in the recent density functional study[19] of the turnstile rotational barrier of the closely related η^4-nbd compound **2**, mentioned in the Introduction. The entropy of activation, evaluated from the Eyring plot, is close to zero ($\Delta S^{\ddagger} = -0.3$ cal·K^{-1}·mol^{-1}) as can be expected for a simple intramolecular rearrangement of a neutral molecule in a nonpolar solvent.

The hypothetical ν(CO) spectra of **1** in the absence of CO site exchange, displayed in Figure 8, illustrate the pure effect of the temperature-dependent modifications in the spectral parameters. The changes with temperature in the band profiles are a bit more pronounced than those observed in the variable-temperature spectra of $Fe(CO)_3(\eta^4$-1,3-butadiene) (**4**) (Figure 5), proven to be rigid on the vibrational time scale. This might well be interpreted in terms of some differences in the intrawell dynamics which, however, would not be too surprising in view of the very flat potential well in the case of $Fe(CO)_3(\eta^4$-1,5-cod) (**1**).

Conclusion and Outlook

Our results convincingly justify the exploitation of vibrational line broadening and coalescence phenomena for the purpose of investigating very fast, reversible reactions with kinetics in the picosecond time domain and accordingly low barriers of

activation. The CO stretching vibrational spectra of carbonyl-metal complexes, with their narrow and well-defined band profiles in the absence of chemical exchange, are ideal for testing the validity of this approach. Noted with great interest, the IR spectra of a series of mixed-valence ruthenium cluster complexes, with two pyrazine-bridged $Ru_3(\mu_3\text{-O})$ cores and one CO ligand attached to each of the subunits, were recently reported to exhibit (partial) coalescence of the ν(CO) bands as a result of rapid intramolecular electron transfer.[38] Reaction rates in the order of 10^{12} s^{-1} were estimated on the basis of line shape simulations by using the program developed in our present study, thus further underlining the value of our approach as a promising tool in such investigations.

Our continued efforts are directed to a comparative investigation into the variable-temperature ν(CO) IR spectra of $Fe(CO)_3(\eta^4\text{-nbd})$ (**2**) (Figure 1) and its ^{13}CO-labeled derivatives. This work will further substantiate the reliability of our approach because of the varying separations in frequency of the coalescing bands in the spectra of the different isotopomers, while the same activation barrier and, accordingly, the same rate constant for the underlying processes (CO/CO, CO/^{13}CO, and ^{13}CO/^{13}CO site exchanges) should be operative. Unfortunately, the lower frequency part of the ν(CO) pattern of $Fe(CO)_{3-n}(^{13}CO)_n(\eta^4\text{-nbd})$ (**2-#**),[4] with *statistical* distribution of the ^{13}CO label, suffers from substantial overlap of a large number of bands in a rather narrow spectral region. Thus, although the temperature-dependent collapse of bands associated with the individual species is recognizable, the subtle details of changes in the line shapes cannot be monitored with sufficient accuracy. In view of this deficit, we have endeavored to develop a synthetic route to the *selective* incorporation of *one* or *two* ^{13}CO groups, which will be published in a forthcoming paper.

Experimental Section

$Fe(CO)_3(\eta^4\text{-1,5-cod})$ (**1**) was photochemically prepared[21] from $Fe(CO)_5$ and 1,5-cyclooctadiene, in analogy to a published procedure.[39] The ^{13}CO-enriched sample $Fe(CO)_{3-n}(^{13}CO)_n(\eta^4\text{-1,5-cod})$ (**1-#**),[7] generated by irradiation of **1** in ^{13}CO-saturated solution and separated from concomitantly formed $Fe(CO)_{3-n}(^{13}CO)_n(\eta^4\text{-1,3-cod})$, was available from a previous study.[21] $Fe(CO)_3(\eta^4\text{-1,3-butadiene})$ (**4**)[27] and $Fe(CO)(\eta^4\text{-1,3-butadiene})_2$ (**5**)[27,29] were photochemically prepared from $Fe(CO)_5$ and 1,3-butadiene in analogy to published procedures. 2-Methylpentane (Merck, synthetic grade) was distilled under argon prior to use. ^{13}CO (CLM-1845: 99% ^{13}C, <1% ^{18}O) was purchased from Cambridge Isotope Laboratories (Promochem, Wesel).

The low-temperature matrix isolation equipment has been described previously,[40] including the setup for wavelength-selective irradiation and the devices for controlling the temperature, the flow of matrix gas (1.5−2 mmol h^{-1}), and the metal complex deposition rate. The evaporation temperature for the samples of **1** and **1-#** (6−8 °C) was adjusted to achieve a guest/host ratio of ≤1/1000. Low-temperature matrix IR spectra were recorded on a Perkin-Elmer 1720 FTIR instrument.

A low-temperature IR cell (1 mm path length, CaF_2 windows), cooled with a flow of nitrogen gas, was used for recording the variable-temperature IR spectra in 2-methylpentane solution on a Bruker IFS 66 FTIR instrument, operating with 9-mm aperture and employing 54K data points, with Blackman-Harris-3Term apodization, giving 1 cm^{-1} resolution.

Acknowledgment. This paper is dedicated to Professor Günther O. Schenck on the occasion of his 85th birthday. The authors thank P. Bayer, G. Klihm, and R. Schrader for their skilled technical assistance. Fruitful discussions with Prof. J. J. Turner (University of Nottingham, U.K.) and Dr. F. Mark (MPI für Strahlenchemie) are gratefully acknowledged. Partial financial support of this work by the EU (HCM program, Contract No. CHRX-CT93-0152) is also acknowledged.

JA973897H

(38) Ito, T.; Hamaguchi, T.; Nagino, H.; Yamaguchi, T.; Washington, J.; Kubiak, C. P. *Science* **1997**, *277*, 660−663.

(39) Deeming, A. J.; Ullah, S. S.; Domingos, A. J. P.; Johnson, B. F. G.; Lewis, J. *J. Chem. Soc., Dalton Trans.* **1974**, 2093−2104.

(40) (a) Klotzbücher, W. E. *Cryogenics* **1983**, *23*, 554−556. (b) Gerhartz, W.; Grevels, F.-W.; Klotzbücher, W. E. *Organometallics* **1987**, *6*, 1850−1856.

(41) The relative intensities of the three ν(CO) bands were kept constant in the simulations, while the absolute integrated intensities were modified with temperature by a factor of 2% in steps of 20 K.

(42) Grevels, F.-W. et al., unpublished results.